

Accepted for publication in the Astrophysical Journal

Deep Photometry of the Globular Cluster M5: Distance Estimates from White Dwarf and Main Sequence Stars

Andrew C. Layden

*Department of Physics and Astronomy, 104 Overman Hall,
Bowling Green State University, Bowling Green, OH 43403*

layden@baade.bgsu.edu

Ata Sarajedini

*Department of Astronomy, 211 Bryant Space Science Center, P.O. Box 112055,
University of Florida, Gainesville, FL 32611*

ata@astro.ufl.edu

Ted von Hippel

*Department of Astronomy, 1 University Station C1400,
The University of Texas at Austin, Austin, TX 78712-0259*

ted@astro.as.utexas.edu

and

Adrienne M. Cool

*Department of Physics and Astronomy, 1600 Holloway Avenue,
San Francisco State University, San Francisco, CA 94132*

cool@sfsu.edu

ABSTRACT

We present deep VI photometry of stars in the globular cluster M5 (NGC 5904) based on images taken with the *Hubble Space Telescope*. The resulting color-magnitude diagram reaches below $V \approx 27$ mag, revealing the upper 2–3 magnitudes of the white dwarf cooling sequence, and main sequence stars eight

magnitudes and more below the turn-off. We fit the main sequence to subdwarfs of known parallax to obtain a true distance modulus of $(m - M)_0 = 14.45 \pm 0.11$ mag. A second distance estimate based on fitting the cluster white dwarf sequence to field white dwarfs with known parallax yielded $(m - M)_0 = 14.67 \pm 0.18$ mag. We discuss the nature of the difference between the two distance estimates and suggest approaches for reducing the uncertainty in white dwarf fitting estimates for future studies. We couple our distance estimates with extensive photometry of the cluster’s RR Lyrae variables to provide a calibration of the RR Lyrae absolute magnitude yielding $M_V(RR) = 0.42 \pm 0.10$ mag at $[\text{Fe}/\text{H}] = -1.11$ dex. We provide another luminosity calibration in the form of reddening-free Wasenheit functions. Comparison of our calibrations with predictions based on recent models combining stellar evolution and pulsation theories shows encouraging agreement, and the existing differences may provide useful feedback to the models.

Subject headings: globular clusters: individual (NGC 5904) — stars: distances — stars: Population II — subdwarfs — white dwarfs

1. Introduction

RR Lyrae variable stars (RRL) are among the most popular standard candles for measuring distances to old stellar populations, both within the Galaxy and to other galaxies in the Local Group. Common targets include Galactic globular clusters, the Galactic Center, the Magellanic Clouds and the dwarf spheroidal companions of the Galaxy, and even M31 and M33 and their companions. The distance scale adopted for the globular cluster system also defines the mean age and age distribution of that system. Globular clusters (GCs) place strong constraints on the chronology of star formation and chemical evolution in the early Galaxy. Also, the age of the oldest GCs places a firm lower limit on the age of the Universe, thus providing an important consistency check on studies determining fundamental cosmological parameters. Clearly, an accurate calibration of the RR Lyrae absolute magnitude, $M_V(RR)$, is vitally important for many fields of astronomy.

Carretta et al. (2000) reviewed the status of this calibration after the results of the *Hipparcos* astrometry satellite had been digested. They compared the results of numerous distance estimation techniques, and found encouraging evidence that the long-standing dichotomy between the long and short distance scales was at last yielding better consistency. Still, evidence persisted that different techniques produced systematically different results. For example, their careful analysis of main-sequence fitting techniques consistently produced

a distance scale about 0.1 mag brighter than the mean of other methods. They also demonstrated that the chief limitation of this technique was the restricted sample of subdwarf stars available with high quality parallaxes. Until another astrometry satellite is launched, it seems unlikely this technique will undergo substantial improvement.

It is therefore worthwhile to explore and develop other techniques for calibrating the RRL luminosity. One technique still in its natal stages is white dwarf (WD) sequence fitting. WD fitting is analogous to main sequence (MS) fitting except that the cluster’s WD cooling sequence is fit to local WDs with trigonometric parallaxes (e.g., Renzini et al. (1996)), and/or theoretical model cooling sequences (e.g., Wood (1995)). WDs possess a number of advantages over MS stars which may result in more trustworthy fits. First, WD atmosphere models in this temperature range involve different physics from MS stars, some of which is simpler: there is no convection involved, and the opacities are dominated by hydrogen or helium. Complexities in WD models such as core composition and crystalization should not produce significant luminosity differences between WDs in globular clusters and the field at the temperature and mass range of interest. The models thus involve a different set of systematic uncertainties with respect to the MS models, and therefore provide a new and independent means for obtaining globular cluster distances. Second, the luminosity of a WD is nearly independent of the star’s initial, MS composition. Thus the large number of disk WDs near the Sun are available as calibrators. The main source of observational uncertainty in WD fits involves WD masses, m_{WD} . The Wood (1995) sequences indicate $\partial M_V / \partial m_{WD} \approx 2.4 \text{ mag } m_{\odot}^{-1}$ at a given color (Renzini et al. 1996). Fortunately, GCs have a very narrow range of masses evolving off the MS feeding the WD track, and various arguments indicate that $m_{WD} = 0.53 \pm 0.02 m_{\odot}$ for GCs (Renzini & Fusi Pecci 1988; Richer et al. 1997). This uncertainty translates into ~ 0.05 mag in distance modulus.

Unfortunately, WDs are extremely faint, so WD fitting has not been pursued extensively. Cool et al. (1996) found the brightest WD in NGC 6397, at $V \approx 23$ mag, ~ 10 mag fainter than the horizontal branch. Accurate WD fits require reasonable photometry (~ 0.1 mag) several magnitudes down the WD sequence, so very deep imaging is required. Significant WD sequences have been uncovered in only a handful of globulars to date (Richer et al. 1995; Elson et al. 1995; Di Marchi & Paresce 1995; Cool et al. 1996; Renzini et al. 1996; Zoccali et al. 2001). Most of these clusters have extremely red or blue horizontal branch (HB) stars, and contain few or no RRL. Any estimates of $M_V(RR)$ based on these clusters require extrapolating the HB across the RR Lyrae pulsation strip. This can be done with the aid of theoretical HB models, but at the cost of the assumptions and uncertainties inherent in those models. The exception, M4, is rich in RRL, but suffers from a high foreground reddening which varies spatially across the cluster and which follows a non-standard reddening law (Richer et al. 1997). This complication translates into substantial uncertainty in any RRL

luminosity calibration thus derived.

The nearest globular with both a low reddening and abundant RRL is M5 (NGC 5904). We have therefore undertaken a project to measure the distance to M5 using WD fitting, and thereby calibrate the luminosity of its RRL. This paper describes our deep imaging of M5 using the *Hubble Space Telescope (HST)*, our photometric analysis procedure and methodology for detecting WDs (Sec. 2), and our distance analyses using both WD fitting (Sec. 3) and main sequence fitting (Sec. 4). In Secs. 5 and 6, we combine these results with extensive photometry of the M5 RRL compiled from the literature to provide RRL luminosity calibrations in several forms. We discuss our results and how they might be improved upon in Sec. 7.

2. Observations and Reductions

Images of a region in M5 were obtained using the *Wide Field and Planetary Camera 2 (WFPC2)* aboard *HST* as part of program GO-8310. The WFPC2 region is located at equatorial coordinates $\alpha = 15^h 18^m 36.00^s$ and $\delta = +02^\circ 08' 18.4''$ (J2000), about 200 arcsec North of the cluster center at a point providing a high surface density of white dwarfs with minimal crowding by bright cluster stars.

Images were obtained using the F555W and F814W filters during four visits to the cluster as described in Table 1. This table includes the date of each visit, the orbit number within the visit, the filter used, and the number and length of exposures obtained during the orbit. The telescope pointing was dithered slightly between orbits two and three of Visits 1, 2, and 3, and between each of the orbits of Visit 4. Shorter exposures were included to provide photometry of brighter stars useful for photometric comparisons with ground based photometry. The total exposure times in F555W and F814W were 13,695 sec and 20,260 sec, respectively, obtained over fifteen spacecraft orbits.

Raw images and optimal calibration frames were downloaded and recalibrated “on the fly” from the Canadian Astronomical Data Centre¹. The resulting calibration employed improved bias and dark files compared with the original calibration provided by the Space Telescope Science Institute.

Rejection of cosmic rays was accomplished using the STSDAS task CRREJ. In each orbit shown in Table 1, cosmic rays were detected in the stack of three long-exposure images by iteratively rejecting deviant intensity values at each pixel location, with the rejection

¹<http://cadwww.dao.nrc.ca/>.

criterion becoming stricter in each iteration. We also tested for cosmic rays in pixels adjacent to known cosmic rays. For each orbit, the result was a mask identifying the location of cosmic rays on each of the three images. The masked F555W images from all six orbits were then shifted and combined using MONTAGE2 (Turner 1996) to produce a high signal-to-noise image with the cosmic rays rejected. Note that in this image, the pixels where cosmic rays were eliminated have a lower signal-to-noise than the pixels which enjoyed uncorrupted data values. In a typical mask for a single image, we found that $\sim 6\%$ of the pixel locations were affected by cosmic rays. Using this cosmic ray rate, we performed a simple statistical model to determine the fraction of WFPC2 pixel locations affected, and to estimate the signal-to-noise degradation caused by cosmic rays to our combined image. About one third of the WFPC2 pixels were unaffected by cosmic rays, while $\sim 38\%$ of the pixel locations suffered a cosmic ray hit in one of the stacked intensity values. In total, $\sim 98\%$ of the WFPC2 pixels were affected by three or fewer cosmic rays, causing a signal-to-noise to drop of at most 9% relative to pixel locations with no cosmic rays. This indicates that the vast majority of the area surveyed has fairly uniform characteristics that should not affect significantly our detection of faint stars. The worst case encountered in the model was when seven cosmic rays hit a particular pixel location, leading to a 22% drop in signal-to-noise relative to unaffected pixels. However, such cases were rare, affecting only ~ 20 pixels across the entire survey area. We conclude that the presence of cosmic rays has had minimal impact on the detection of faint stars. As we will show in the following section, detection incompleteness due to crowding is significantly more important.

2.1. Object Finding and Photometry

We used SExtractor (Bertin & Arnouts 1996) to find and classify sources on the final, combined F555W image. The resulting list of object positions was used as input to ALLFRAME (Stetson 1994) to perform point spread function (PSF) fitting photometry on the individual, cosmic ray-masked F555W and F814W frames. Each frame was first multiplied by a geometric correction frame obtained from the *HST* Archive to correct for distortions in the apparent area of pixels produced by the WFPC2 cameras. Experimentation with the tunable parameters in ALLFRAME and SExtractor was done to optimize extraction of the faint WD candidate stars in our frames. The high signal-to-noise *HST* PSFs for F555W and F814W that were utilized in the reduction of *HST* images by the Cepheid Distance Scale Key Project team (Silbermann et al. 1996, kindly provided by Peter Stetson) were applied to each of our 59 frames. Positional transformations between each frame and a reference image were used by ALLFRAME to simultaneously iterate on the positions and magnitudes of each object supplied by SExtractor. The result was profile-fitting photometry for approximately

8000 sources in each of the long exposure WF frames. We did not perform photometry on the PC images since the small area of sky covered by that chip would yield very few WD stars.

Besides using SExtractor to find objects in the WFPC2 frames, we also retained the “class” parameter computed by SExtractor. While not strictly a Bayesian classification, the value of class is approximately the probability that any given object is stellar, with 1.0 representing definite unresolved sources, and 0.0 representing definite non-stellar sources. We will return to the use of this morphological information below, when we discuss cleaning the color-magnitude diagram.

We then reapplied SExtractor to find additional faint sources on the PSF-subtracted images produced by ALLFRAME. However, inspection of the images showed that many detections were of residual light where the PSF had been imperfectly subtracted from the undersampled profile of an object detected in the first application of SExtractor. Furthermore, a high fraction (79%) of these objects were classified as non-stellar by SExtractor. Though we ran these additional objects through ALLFRAME to determine magnitudes for them, further tests (see Sec. 2.3) indicated that they would add to our data set many false detections and few stars upon which high-quality photometry could be done. Therefore, we report magnitudes only for the objects detected in the first application of SExtractor. We note that the second application of ALLFRAME photometry did help to improve the photometry of the stars found in the first pass by accounting for, at least approximately, the light from nearby, fainter objects.

2.2. Calibrating the Photometry

At this point, we followed the procedure outlined by Sarajedini et al. (2000) to obtain aperture corrections which convert our instrumental, PSF-fitting photometry from ALLFRAME into the equivalent aperture magnitudes via a zeropoint offset. We then applied the Silberman et al. (1996) transformation equations to convert our instrumental aperture magnitudes from the F555W and F814W filters into calibrated V and I photometry (respectively) on the scale of Silberman et al. (1996), which represents the work of the *HST* Cepheid Key Project.

We then corrected for a number of well-known photometric effects in the WFPC2 system. As recommended by the WFPC2 Instrument Team, time-dependent corrections for charge-transfer efficiency (CTE) effects were installed based on the prescription of Dolphin (2000),

updated using the data available on his web site². The CCD dewar window throughput also changes as a function of time. After carefully examining the effect of adding these small (-0.002 to $+0.012$ mag), photometric offsets, we determined that the main sequences in the three different WF chips were less aligned with the corrections than without, so we did not apply these corrections. Had we applied these corrections, their effect would have been anyway small, with a maximum of $+0.007$ mag in the V -band, and a maximum of $+0.006$ mag in $V - I$.

Table 2 contains data on all the objects detected on the three WF chips by the first application of SExtractor. The first column contains an identification number generated by ALLFRAME, the second column indicates upon which chip the object fell (WF2, WF3, or WF4), and the next two columns indicate the object’s X and Y pixel coordinates on that chip. Columns 5–8 show the V and I magnitudes and their errors (specifically, the frame-to-frame standard error of the mean, propagated through the photometric transformation equations of Silbermann et al. (1996)). The remaining columns present the SExtractor parameters describing the ellipticity of the object, its full-width at half-maximum in pixels, and the object’s morphological “class” value. The electronic file contains data for 10,409 objects.

2.3. Cleaning the CMD

Figure 1a shows the color-magnitude diagram (CMD) for all objects listed in Table 2. The curves represent the $\log(g) = 7.5$ and 8.0 WD cooling tracks from Bergeron et al. (1995), shifted to account for typical reddening and distance modulus values for M5. These tracks are meant only to guide the eye in finding the CMD location of cluster WDs, and are not used in our WD fitting analysis (Sec. 3). Clearly, the large number of objects spread throughout the middle and blue side of Figure 1a makes it difficult to determine whether WDs are present.

We employed the morphological “class” criterion of SExtractor to statistically reject objects that did not have stellar profiles. After experimenting with morphology cuts, we found that keeping only objects with class > 0.75 gave the greatest reduction in non-stellar objects while retaining most stellar objects. The exact cut value did not matter greatly, and higher class values (greater probability of the object being stellar) gave similar results. The resulting CMD is presented in Figure 1b.

²http://www.noao.edu/staff/dolphin/wfpc2_calib/, updated 2002 Sept. 17.

We note that the number of blue objects scattered between the WD and MS regions in Figure 1b would be much higher had we included the objects detected in the second application of SExtractor (to the PSF-subtracted image) discussed in Sec. 2.1. A CMD of these objects contains a much higher fraction of blue objects relative to MS objects than is seen in Figure 1b (29% and 2%, respectively), and only 1–2 objects fell near the (Bergeron et al. 1995) WD tracks. The vast majority of these sources were faint objects in the wings of brighter stars that were found in the first application of SExtractor. Since our goal is to obtain the highest quality photometry possible, and does not require a high degree of completeness, our purposes are best served by omitting these stars from the CMD.

The cleaned CMD shown in Figure 1b has a narrow, well-defined main sequence extending from just above the MS turn-off to over eight magnitudes below the turn-off. A few dozen WD candidates can be seen in the region around the model cooling tracks. This number agrees with expectations calculated from the number of stars evolving off the MSTO in Figure 1, by way of the evolution rate determined from isochrones (Girardi et al. 2002) and the WD cooling rate (Bergeron et al. 1995). Such calculations are rough given the small number of stars involved and the uncertain degree of detection completeness suffered by the WD and MSTO stars. Still, the agreement between the observed and expected number of WDs in Figure 1b indicates that we are not missing a large fraction of the WDs due to over-aggressive cleaning of the CMD. Most of the blue objects scattered between the WD and MS regions in Figure 1b can be attributed to distant, unresolved galaxies. Using statistics from the Hubble Deep Fields (Williams et al. 1996; Casertano et al. 2000), we expect there to be roughly 33 to 39 unresolved background galaxies with $V < 27$ mag in our CMD. This number is slightly less than the number of blue objects seen in Figure 1b, suggesting that the latter may include some field stars located behind the cluster in the Galactic halo.

2.4. Final Photometry

The errors presented in columns 6 and 8 of Table 2 indicate the internal, random errors associated with our photometry. We determined typical error values for stars in specific regions of the CMD shown in Figure 1b by computing the median uncertainties in V and $V - I$ within selected magnitude and color ranges. At $V \approx 21$ mag, the median errors in V and $V - I$ are 0.015 and 0.019 mag, respectively. They gradually increase at fainter magnitudes, reaching 0.056 and 0.061 mag for stars at the lower end of the MS, and 0.051 and 0.098 mag in the WD region. The internal errors for stars brighter than $V \approx 21$ mag increase to ~ 0.036 and ~ 0.047 mag because lower signal-to-noise photometry was included from a few short exposure WFPC2 images.

To obtain an estimate of the external, transformation-based errors in our photometry, we compared our final WFPC2 photometry with the M5 standard fields observed by Stetson (2000). For the fifteen bright stars in common between the two datasets, we find offsets of $V_{us} - V_{Stetson} = -0.053 \pm 0.010$ and $I_{us} - I_{Stetson} = -0.059 \pm 0.009$ mag, with no correlation with color or magnitude. While the zeropoint differences in the magnitude scales are statistically significant, it is gratifying to find that the $V - I$ color scales are essentially identical. We note that these fifteen stars are among the brightest in our data set. They were derived from short exposure images and may not accurately represent the photometry of WD and lower MS stars, derived from the long-exposure images, about eight magnitudes fainter. Since it is not evident which zeropoints are correct, we have chosen *not* to apply these magnitude offsets to our photometry. Instead, we will quote our distances with and without these offsets.

It is instructive to obtain a sense of the depth of our photometry in terms of the physical properties of low-luminosity stars. We estimate the mass of the faintest main sequence stars visible in our photometry by comparing with the isochrones of Girardi et al. (2002). A slight extrapolation below the low-mass limit of the isochrone with $Z = 0.001$ and age of 14.1 Gyr suggests the MS stars at our photometric limit of $V = 27$ mag have masses of about $0.14 m_{\odot}$. Though our photometry is deep, we are not reaching the MS hydrogen burning limit, which is predicted by some models to be ~ 8 mag below the faintest MS stars in our data set. Nor are we reaching the lower limit of the WD cooling sequence expected at $V > 31$ mag, or the WD luminosity function jump created by the changing atmospheric opacity due to neutral hydrogen expected at $V \approx 29.5$ mag (Hansen et al. 2004). While our data is not suited to examining the transition between lower MS and brown dwarf stars or determining the age of M5 from its WD stars, it is well suited for its intended purpose: a distance estimate to M5 based on WD fitting.

3. White Dwarf Fitting Distance

Figure 1b presents a distinct sequence of several dozen WD candidates running from $V \approx 24$ mag to the limit of the photometry at $V \approx 27$ mag. We zoom in on the WD region in Figure 2. We restrict our WD distance analysis to stars with $V < 26$ mag to minimize bias due to incompleteness near the limit of our photometry, and to minimize uncertainty as the errorbars increase with magnitude. We inspected the F555W and F814W images at the locations of the 27 cluster WD candidates in Figure 2. Most candidates are isolated and should not be subject to systematic photometry errors due to crowding. There are several marginal cases worth noting, however. The star at $(V - I, V) = (-0.32, 25.10)$ is located near

a brighter star whose diffraction spike probably compromises our photometry. The stars at $(-0.21, 24.38)$, $(+0.27, 25.12)$, and perhaps $(-0.25, 25.26)$ may also have crowding-related errors. We placed less weight on these stars in our analysis as described below.

Zoccali et al. (2001) determined a distance to the globular cluster 47 Tuc by matching WFPC2 photometry of local WDs which have known masses and trigonometric parallaxes to WFPC2 photometry of likely WDs in 47 Tuc. In order to avoid dependencies on the assumed photometric transformations, Zoccali et al. compared the local and 47 Tuc WD samples in the instrumental magnitude system, after incorporating the Dolphin (2000) CTE corrections. Zoccali et al. also corrected each of the local WD calibrators to a WD mass of $0.53 M_{\odot}$, the assumed mass value of the WDs observed in 47 Tuc. In order to be as consistent as possible with their technique, we made a small correction to their local WD instrumental magnitudes (kindly provided by M. Zoccali) for the difference in CTE corrections they used and the more updated CTE corrections currently supplied by Dolphin. We determined updated CTE corrections for the field WDs by downloading the WFPC2 observations from the *HST* archives, then measuring the WD fluxes and surrounding sky values for each frame. The CTE corrections under the two Dolphin prescriptions were computed and compared to each other. The difference in the two corrections only amounts to 1%, in the sense that the Dolphin (2000) correction is 1% larger than the more modern correction, specifically 0.0013 mag compared to 0.0003 mag, for these particular WDs. Finally, we applied the Silbermann et al. (1996) photometric transforms to the field WDs to put them on the same scale as our M5 WDs. This is equivalent to removing the Silbermann et al. photometric transform from the GC WDs and determining distance in the instrumental magnitude system, as done by Zoccali et al. Table 3 presents our final photometry for the DA WDs found in Table 1 of Zoccali et al. (2001).

As done by Zoccali et al. (2001), a straight line was fit to the final photometry for the field WD sample, and then this line was fit to the GC WDs within the same color range ($V - I = -0.226$ to $+0.002$, i.e., without consideration of error bars). This narrow requirement for inclusion was chosen for this first iteration on determining the M5 WD distance both to avoid extrapolation and to omit stars with photometry possibly contaminated by crowding. To accomplish the fitting, we used GaussFit, a code for least squares and robust estimation (Jefferys et al. 1988), which allowed us to fully incorporate uncertainties in the colors and magnitudes, the covariance between color and magnitude, and the uncertainty in the slope of the fit to the field WD sequence. The resulting distance modulus was 14.70 ± 0.12 mag. In a slightly different approach, using the same data but without the single most deviant (brightest) object, we simultaneously fit a single slope and two intercepts for the field WD and M5 WD data. This yielded a distance modulus of 14.85 ± 0.32 mag. Figure 2a presents the WD region of the CMD, including the calibrating field WDs (triangles) and the M5 WDs

used (open circles) in these fits, and demonstrates why these two nearly identical procedures might give significantly different uncertainties. The error bars for the field WDs are large due to the combined uncertainties in their photometry, trigonometric parallaxes, and the corrections required to transform them to the comparison mass of $0.53 M_{\odot}$. The calibrating WDs also appear to form a steeper sequence than the cluster WDs. The steepness and scatter along the sequence is most likely due to small differences in mass; either real mass differences in the case of the M5 WDs, or small errors away from the corrected mass values for the calibrating WDs. It is also possible that some of the M5 WDs are He-atmosphere WDs, in which case they should be 0.02 to 0.07 mag bluer (Bergeron et al. 1995) than the WD calibrating sequence.

We iteratively improved on this preliminary WD distance for M5 by placing the calibrating WDs back in the CMD (see Figure 2b) and reselecting the individual WD candidates. This time, instead of selecting cluster WDs based solely on their color, we selected WDs based on both magnitude and color. Specifically, we included in the fits all WD candidates whose $1\text{-}\sigma$ error ellipses in the CMD overlapped with the sequence defined by the local WD sample. This two-parameter cut had the effect of dropping the brightest WD candidate and including two other fainter WD candidates. Figure 2b shows that it also selected against the stars with questionable photometry. The two statistical approaches tried above (imposed slope and simultaneous fit) yielded distance moduli of 14.77 ± 0.11 and 14.79 ± 0.26 mag, respectively. These improved distances are within the errors of the distances derived initially, and are slightly preferred on sample-selection grounds.

While the agreement of the two values is encouraging, the discrepancy in the uncertainties highlights the sensitivity of the results to the adopted fitting procedure. As a conservative compromise, we adopt $(m - M)_V = 14.78 \pm 0.18$ mag as our estimate of the distance modulus for M5 as derived from its WD stars.

4. Main-Sequence-Fitting Distance

Our deep photometry of M5 provides us with an opportunity to determine the cluster’s distance by fitting its MS to nearby subdwarfs with known trigonometric parallaxes. A number of inputs are required, including a fiducial sequence for the MS region of the cluster, a set of subdwarf stars with known metallicities and trigonometric parallaxes, and a prescription for adjusting the colors of the subdwarfs for the effects of metallicity.

The main sequence fiducial has been constructed in the following manner. We divided the data into bins of 0.2 mag between $V = 18.5$ and $V = 26.1$ mag. Within each bin, we

compute the median color of all stars and then perform a 1σ rejection until the median color difference from iteration to iteration is less than 0.005 mag. The resultant fiducial sequence, shown in Figure 3a, does not appear to be influenced by the unresolved binaries which lie above and to the right of the MS.

The set of subdwarf stars has been taken from the work of Sandquist et al. (1999) as listed in their Table 4. All of these stars possess *Hipparcos* parallaxes and their absolute magnitudes have been corrected for the Lutz-Kelker bias as described in Sandquist et al. (1999). All but one of these stars has a more recent metallicity determination from the work of Gratton et al. (2003). The mean difference in metallicity is 0.09 ± 0.03 dex in the sense (Sandquist – Gratton). For the one star without a Gratton et al. metal abundance measurement (BD +54 1216), we offset the Sandquist et al. value by -0.09 dex to account for the different abundance scales.

The colors of the subdwarf stars are adjusted for their metallicity using the Girardi et al. (2002) isochrones for $Z=0.00001, 0.0004, 0.001, 0.004, 0.008, \text{ and } 0.019$ in the range $4.5 < M_V < 8.0$ mag. We have parameterized the $V-I$ colors of these models along the MS as a function of M_V and $[\text{Fe}/\text{H}]$. Then, the partial derivative of this relation $(\partial(V-I)/\partial[\text{Fe}/\text{H}])$ is used to adjust the subdwarf colors to the metallicity of M5, which we take to be $[\text{Fe}/\text{H}] = -1.11 \pm 0.03$ (Carretta & Gratton 1997).

With the above-mentioned points in mind, and adopting a reddening to M5 of $E(V-I) = 0.046 \pm 0.020$ mag (see Sec. 6), we performed a weighted least squares fit of the M5 MS fiducial to the metallicity-adjusted subdwarf photometry taken from Table 4 of Sandquist et al. (1999). The resultant fit, shown in Figure 3b, yields an apparent V -band distance modulus of $(m-M)_V = 14.56 \pm 0.10$ mag. The error was computed from the uncertainty due to reddening (~ 0.10 mag), the standard error of the subdwarfs around the fitted fiducial (~ 0.01 mag), and the effect of a random metallicity error of 0.03 dex on the results of the fit (~ 0.01 mag). Correction for interstellar extinction results in a true distance modulus of $(m-M)_0 = 14.45 \pm 0.11$ mag, which includes the additional error inherent in A_V .

Our value for the distance modulus of M5 is in good agreement with the MS fitting result of Testa et al. (2004), who found $(m-M)_0 = 14.44 \pm 0.09$ (random) ± 0.07 (systematic) mag. Other recent main sequence fitting results for M5 yielded true distance moduli of 14.46 ± 0.05 mag (Carretta et al. 2000), 14.52 ± 0.15 mag (Reid 1998), and 14.42 ± 0.09 mag (Chaboyer et al. 1998). Much of the uniformity between these results arises from the sample of subdwarfs employed, which is defined by the availability of parallaxes from the *Hipparcos* satellite. Subtle differences between them include the photometric zeropoints, which subdwarfs were used, and the way in which the colors of the subdwarfs were corrected for metallicity effects. If we apply the offset to our photometry indicated by Stetson (2000)

ground-based photometry (see Sec. 2.4), our value becomes $(m - M)_0 = 14.50 \pm 0.11$ mag.

5. Apparent Magnitudes of the RR Lyrae

Having established estimates for the distance modulus to M5, we can provide a calibration of the RR Lyrae absolute magnitude, $M_V(RR)$. This requires a careful measurement of the mean apparent V magnitude of the ensemble of RRL in M5, $V(RR)$. The RRL themselves do not appear in our *HST* data, so we rely on ground-based observations compiled from the literature. Photometry in the B , I , and K passbands are also available in the literature, enabling us to calibrate the RRL absolute magnitude in these bandpasses as well. We note that systematic zeropoint differences may exist between these sources and our photometry (in Table 2, or if corrected to the Stetson (2000) system). Such problems are common in $M_V(RR)$ calibrations like MS fitting where the deep MS photometry and shallow time-series photometry of the RRL are often obtained by different researchers using different detectors, standard stars, etc.

Light curves for RRL in M5 are presented in several studies, including Brocato, Castellani & Ripepi (1996, B and V magnitudes); Caputo et al. (1999, B and V); Cohen & Matthews (1992, K); Kaluzny et al. (1999, V); Longmore et al. (1990, K); Reid (1996, V and I); Storm, Carney & Beck (1991, B and V); and Storm, Carney & Latham (1992, K). To ensure self-consistency of our statistics, we took the light curves of each star from their original source and recomputed the star’s intensity-mean magnitude, $\langle m_i \rangle$, separately in each filter (B , V , I , and K). This entailed converting the individual magnitude estimates in a light curve into intensity estimates, integrating under the phased light curve, and converting the resulting mean intensity back into a magnitude. We rejected any star with a phase gap large enough to bias the estimate of $\langle m_i \rangle$. The resulting intensity-mean values are shown in Figure 4 as a function of each star’s pulsation period.

Four studies provide V magnitudes. We compared the $\langle V_i \rangle$ estimates for stars common to different pairs of studies to search for any systematic differences in photometric zero-points between the studies. Differences of order 0.02 mag were found, but they appeared to reflect the sub-samples of stars involved more than systematic photometric differences. We therefore took the $\langle V_i \rangle$ values at face value. If, for a given star, $\langle V_i \rangle$ values were available from more than one study, we averaged the values together to get a mean value for the star. In this way, we compiled a list of 79 RRL including 53 RRab and 26 RRc.

Figure 4b shows the $\langle V_i \rangle$ value for each star plotted against the star’s period. Statistics on this sample is shown in the first row of Table 4. The columns in this table give the

number of stars used in the sample (N_{RR}), the arithmetic mean of the $\langle m_i \rangle$ values $m(RR)$, the standard error of the mean (sem), the standard deviation about the mean (σ), and the median of the $\langle m_i \rangle$ values ($median$). The table presents separate statistics for RRab and RRc variables, though in V there is no significant difference between the mean magnitudes of the RRab and RRc stars. We adopt $V(RR) = 15.024 \pm 0.009$ mag as the mean apparent magnitude of the 79 RRL studied in M5. The error estimate reflects the observed scatter in the stellar magnitudes, while a systematic uncertainty of $\lesssim 0.02$ mag can be expected in the photometric zeropoint. For comparison, Harris (1996)³ lists the HB magnitude of M5 to be 15.07 mag. The lower envelope of the distribution of the points in Figure 4, which should correspond to the Zero-Age Horizontal Branch locus, is at 15.10 ± 0.04 mag.

We compiled B -band data from the three sources listed above. There were no stars in common between the three studies, so no star-by-star analysis was possible and no systematic zero-point corrections were made. Figure 4a shows the $\langle B_i \rangle$ value for each star plotted against the star’s period. The statistics for RRab and RRc considered separately (see Table 4) indicate that the RRc stars in M5 are significantly brighter than the RRab stars. The mean apparent B -band magnitude of the combined sample of RRL in M5 is $B(RR) = 15.350 \pm 0.018$ mag. As for V , the error estimate reflects the observed scatter, while a systematic error of $\lesssim 0.02$ mag is possible in the photometric zeropoint.

Light curves in the I -band are available only from one source (Reid 1996). The statistics shown in Table 4 indicate that the RRc stars are significantly fainter in I than the RRab stars, i.e., in the sense opposite to that of the B filter. Furthermore, Figure 4c shows a strong correlation between I magnitude and period among the RRab stars. This period-luminosity correlation is well-known in redder passbands such as K (e.g., Longmore et al. 1990). To characterize this correlation, we fundamentalized the periods of the RRc stars ($\log P_f = \log P_{RRc} + 0.13$, Castellani & Quarta (1987)), and performed a least squares fit to all the RRL data using an equation of the form

$$I(RR) = a + b (\log P_f + 0.3).$$

Line 1 of Table 5 presents the fitted coefficients and their uncertainties, the rms scatter of the points about the fit, and the number of points used in the fit. This relation may be subject to a systematic zeropoint uncertainty of $\lesssim 0.02$ mag.

Light curves in the K -band are available from three studies. Both Cohen & Matthews (1992) and Storm et al. (1992) provided well-sampled light curves for small numbers of stars (four and two, respectively) calibrated to the CIT standard system of Elias et al. (1982).

³Data taken from the 1999 June 22 update available at <http://physun.physics.mcmaster.ca/~harris/mwgc.dat>.

Longmore et al. (1990) took the opposite approach, obtaining only 1–2 observations per star for 23 separate stars. This yields a larger sample of stars, but with increased scatter (rms ≈ 0.05 mag) around a true mean relationship due to phase-sampling effects. Also, the Longmore et al. (1990) data are not directly calibrated to the Elias et al. (1982) standards, though the authors argue there should be no systematic offset. Figure 4d shows the $\langle K_i \rangle$ value for each star plotted against the star’s period, and Table 4 provides statistics. There is evidence for discrepancies in the photometric zeropoints of the three studies at the 0.05–0.10 mag level, though there are too few stars in common to determine any such shifts with accuracy. Normally, the K -band luminosity of RRL is characterized as a function of period. The scatter in the Longmore et al. (1990) data results in uncertainty in the period-dependence derived from Figure 4d. To reduce this uncertainty, we adopt the mean period-dependence (gradient) of the eight clusters presented in Table 4 of Longmore et al. (1990), and fit it to the $\langle K_i \rangle$ data for the four stars with complete light curves using an equation analogous to the one for $I(RR)$ above. Line 2 of Table 5 shows the results of the fit. We estimate the systematic uncertainty in the zeropoint of this relation to be ~ 0.07 mag. Clearly, well-sampled K -band light curves for many RRab and RRC in M5 are needed to ensure a definitive K -band luminosity calibration for M5.

6. RR Lyrae Luminosity Calibration

To obtain a final calibration of the RR Lyrae absolute magnitude, $M_V(RR)$, we must combine our distance modulus and apparent magnitudes with interstellar extinction information. From the WD distance analysis, we obtained an apparent distance modulus of $(m - M)_V = 14.78 \pm 0.18$ mag, while the main sequence fitting analysis yielded $(m - M)_V = 14.56 \pm 0.10$ mag. We are encouraged by the agreement of the results relative to their formal errors. We combined the two results via a weighted mean, using the inverse-squared errors for the weights, to obtain a single estimate of the apparent distance modulus toward M5: $(m - M)_V = 14.61 \pm 0.09$ mag. Clearly, the main sequence fit dominates the combined result.

Testa et al. (2004) advocated the reddening value $E(B - V) = 0.035 \pm 0.005$ mag for M5. We adopt this value along with a more conservative uncertainty of 0.01 mag, which we believe provides a more realistic assessment of the systematic zeropoint uncertainty in the reddening scale (see Sec. 7.4 of Schlegel et al. 1998). This leads to a true distance modulus of $(m - M)_0 = 14.50 \pm 0.10$ mag. We note that the main sequence fitting result is subject to a small systematic uncertainty due to the zeropoint disagreement between our photometry and that of Stetson (2000). The WD value was obtained using photometry of the field

and M5 WDs on the *HST* instrumental system, so should not suffer from this uncertainty. If we shift our photometry to match Stetson’s calibration, the combined distance modulus becomes $(m - M)_0 = 14.54 \pm 0.10$ mag.

Using the relations of Cardelli et al. (1989, their Table 3) in conjunction with our adopted value of $E(B - V) = 0.035 \pm 0.010$ mag, we determine the interstellar extinction values to be $A_B = 0.145 \pm 0.044$ mag, $A_V = 0.109 \pm 0.031$ mag, and $A_K = 0.012 \pm 0.004$ mag. We note that the *I* filter referred to in Cardelli et al. (1989) has a longer effective wavelength than the Kron-Cousins *I* filter, to which the *HST* photometric transformations are calibrated (Silbermann et al. 1996). Using transmission curves of the CTIO I_{KC} filters,⁴ we obtain $A_I = 0.58A_V$ and therefore $A_I = 0.063 \pm 0.018$ mag in the case of M5. Note that this relation yields $E(V - I) = 1.30E(B - V)$, in good agreement with the Kron-Cousins reddening relation described by Dean et al. (1978). We adopt an increased uncertainty in $E(V - I)$ of 0.02 mag to reflect the uncertainty in the reddening relations.

Combining these extinction values with the apparent magnitudes from Table 4 and the true distance modulus, we obtain the absolute magnitudes given in the last column of Table 4, $M(RR)$. We include separate values for RRab and RRC stars. The calibrations corresponding to lines 1 and 2 of Table 5,

$$M(RR) = a + b (\log P_f + 0.3),$$

are shown in lines 3 and 4 of that table, in which the quoted errors include the systematic uncertainties due to the distance modulus and to the photometric zeropoints discussed in Sec. 5. The $M(RR)$ values in Table 4 become 0.04 mag brighter if we adopt the Stetson (2000) photometric system.

Another approach to representing the luminosity of RR Lyrae stars is through the Wasenheit functions (e.g., Kovacs & Walker 2001, Cassisi et al. 2004, and references therein). This reddening-free quantity is especially useful in regions where the reddening is high and varies on small spatial scales. Our high quality distance modulus and RR Lyrae photometry for M5 provide an opportunity to derive an empirical calibration of the Wasenheit functions. This is of particular interest since theoretical calibrations have recently become available through the evolution and pulsation modeling of Cassisi et al. (2004). Additional empirical calibrations may provide useful feedback to the models.

We follow the studies mentioned above in defining the Wasenheit functions $W(BV) = V - R_V(B - V)$ and $W(VI) = V - R_I(V - I)$, where R is the ratio of total absorption

⁴See <http://www.ctio.noao.edu/instruments/filters/index.html>.

to color excess in the appropriate passbands. While both studies adopt $R_V = 3.10$, Kovacs & Walker (2001) employ $R_I = 2.5$, while Cassisi et al. (2004) use 2.54, and we obtain 2.39 from our analysis of the CTIO I_{KC} filter transmission curves. We also define $W(VK) = K - R_K(V - K)$ with $R_K = 0.13$ for use with our compiled K -band data set. Each of these apparent values can be converted to an absolute one via our true distance modulus, $W_0 = W - (m - M)_0$.

Figure 5 shows the W_0 values for our compiled RRL data plotted as a function of fundamentalized pulsation period. The solid line in each panel indicates the least-squares fits to the data in the form

$$W_0 = a + b (\log P_f + 0.3).$$

The fitted coefficients and their errors are given in Table 5 along with the rms scatter of the points about the fit, the number of points in the fit, and the adopted value of R . The error in the coefficient a is a quadratic combination of the error in the fit (typically 0.01–0.03 mag) and the error in the M5 distance modulus (0.10 mag). The values of the a coefficient would become 0.04 mag smaller if we employed the distance modulus appropriate to the Stetson (2000) photometric zeropoint. Notice that in each panel of Figure 5, the stars with complete light curves (solid points) cluster around the fitted line, while stars with phase gaps in their light curves (open symbols) are more often outliers.

In panels (a) and (b), the dashed lines indicate the relation predicted by Cassisi et al. (2004) for their model having metallicity ($Z = 0.001$) and horizontal branch type (+0.11) closest to the observed values for M5. For $W_0(BV)$, our slope is significantly steeper than the predictions (2.5σ), while our zeropoint is only 1.6σ brighter than the predictions owing to systematic uncertainty in the level of the points due to the distance modulus uncertainty. The star-to-star dispersion is also larger than predicted, suggesting that there may be more star-to-star variation in properties such as stellar mass than is expressed in the models. We note that the observational work of Kovacs & Walker (2001) found a slope of -2.47 , in better agreement with the models.

For $W_0(VI)$, the agreement between our observations and predictions appears better (see Figure 5b), with the slope and zeropoint deviating by 0.2σ and 0.6σ , respectively. If we adopt $R_I = 2.54$ to match Cassisi et al. (2004), the points in Figure 5b shift upward and the slope steepens, giving the fitted coefficients shown in line seven of Table 5. Still, the agreement is better than with $W_0(BV)$, showing differences from the predictions by only 1.1σ and 1.3σ for the slope and zeropoint, respectively. The scatter is also smaller, in better agreement with the predictions. The slope of the observed RRL becomes steeper if we convert our intensity magnitudes to the static magnitudes used by the models (Marconi et al. 2003).

Cassisi et al. (2004) discuss the strengths and weaknesses of their models. They note that the slope predictions derive from the relation between pulsation period and stellar luminosity and effective temperature. These relatively well-established elements of the modeling should result in slope predictions that are reliable. Meanwhile, the predicted zeropoints depend on elements of the models that are less constrained (the luminosity of the horizontal branch models and the bolometric corrections), so are less secure. It appears that the input parameters to the models, or perhaps the models themselves, could be adjusted to provide steeper slopes and brighter zeropoints to provide a better match to our observations of M5.

7. Conclusion

We have presented deep *HST* observations of the globular cluster M5. The data reach over eight magnitudes below the main sequence turn-off and include a number of cluster white dwarf stars. By fitting our deep main sequence to a sample of subdwarfs having trigonometric parallaxes, we obtain an apparent distance modulus of $(m - M)_V = 14.56 \pm 0.10$ mag, in good agreement with other main sequence fitting solutions for M5. If the true metallicity of M5 is different from the adopted value of $[\text{Fe}/\text{H}] = -1.11$ dex, the distance modulus shifts systematically by 0.4 mag/dex.

We also described our approach for selecting a sample of WDs with the best quality photometry, and for obtaining a distance estimate to the cluster based on comparison with field WDs having trigonometric parallaxes. The resulting distance modulus, $(m - M)_V = 14.78 \pm 0.18$ mag, is in good agreement with other estimates for M5, indicating that our method is reliable. However, the uncertainty in our WD distance modulus is large compared with the uncertainties associated with more established methods like main sequence fitting.

Much of the uncertainty in our WD distance modulus is attributable to the extreme depth of the observations ($V \approx 25$ mag) in the WD region, and the correspondingly low signal-to-noise of our WD magnitude and color measurements. Newer instruments on *HST* provide better throughput than WFPC2, so could provide higher signal-to-noise at this magnitude. We also note that $V - I$ does not offer the best WD sequence for distance estimation; bluer filters and longer color baselines would result in a WD sequence with a shallower slope. However, the relatively low blue throughput of WFPC2 demanded that we work in the F814W (“*I*”) filter for our study. Another advantage the newer *HST* instruments have over WFPC2 is their superior spatial resolution, which would provide SExtractor with more information to separate WDs from critically resolved, blue background galaxies. Three filter photometry would also help in this separation, as it would with separation of cluster WDs from blue field subdwarf stars. Finally, a second visit to M5 using WFPC2 or one of

the advanced imagers on *HST* would provide both higher signal-to-noise magnitudes, and an opportunity to reject field stars and background galaxies using proper motion information (King et al. 1998). Observations of additional fields in M5 would provide a larger sample of WDs, which would also lead to an improved WD-based distance estimate.

We combined our main sequence and WD results to obtain a best estimate for the true distance modulus of M5: $(m - M)_0 = 14.50 \pm 0.09$ mag. This result is weighted strongly toward the main sequence fit result. Using this in conjunction with a large sample of RR Lyrae magnitudes compiled from the literature, we obtained a calibration for the RR Lyrae absolute magnitude $M(RR)$ in the B , V , I , and K passbands (see Tables 4 and 5). Our value of $M_V(RR) = 0.42 \pm 0.10$ mag is brighter than the value of 0.64 ± 0.07 mag advocated by Carretta et al. (2000) for $[\text{Fe}/\text{H}] = -1.11$ dex. This is consistent with their finding that main sequence fitting calibrations tend to be about 0.1 mag brighter than the average value derived from many independent techniques. The distance modulus obtained from our WD fit would yield $M_V(RR)$ closer to the Carretta et al. (2000) value.

We also presented period-luminosity calibrations in the form of reddening-free Wasenheit functions. These are useful both for distance estimation to heavily reddened systems and for comparison with predictions of recent models that combine evolution and pulsation theories (Cassisi et al. 2004). Our empirical calibration suggests that the current models predict a period dependence that may be too weak and a luminosity zeropoint that may be too faint. However, the systematic over-brightness of main sequence fitting (Carretta et al. 2000) tends to compensate, bringing the theoretical and observed zeropoints into closer agreement.

We conclude that large aperture telescopes with blue-sensitive imagers will enable the WD fitting technique to become increasingly valuable in helping to refine the RR Lyrae luminosity calibration, both for M5 and other globular clusters rich in RR Lyrae stars.

The authors thank an anonymous referee and Marco Castellani for valuable comments and suggestions. We thank Peter Stetson for kindly providing us with PSFs for *HST* F555W and F814W images, Manuela Zoccali for providing us with her instrumental photometry of local field WD stars, Barbara McArthur for help with GaussFit, and Andrew Dolphin for providing CTE correction updates on his website. We also thank Janusz Kaluzny, Vincenzo Ripepi, and Jesper Storm for sending electronic files containing the data from their photometric observations of M5, and Andy Ruggiero for sending us electronic files containing the Reid (1996) RRL light curves. ACL, AS, and TvH acknowledge support from NASA/STScI through grant number HST-GO-08310-97A. TvH gratefully acknowledges support by NASA through LTSA grant 02-0045-0082. Guest User, Canadian Astronomy Data Centre, which is operated by the Herzberg Institute of Astrophysics, National Research Council of Canada.

The Digitized Sky Surveys were also used in the course of this research.

REFERENCES

- Bergeron, P., Wesemael, F., & Beauchamp, A. 1995, *PASP*, 107, 1047
- Bertin, E., & Arnouts, S. 1996, *A&AS*, 117, 393
- Brocato, E., Castellani, V. & Ripepi, V. 1996, *AJ*, 111, 806
- Caputo, F., Castellani, V., Marconi, M., & Ripepi, V. 1999, *MNRAS*, 306, 815
- Cardelli, J. A., Clayton, G. C., Mathis, J. S. 1989, *ApJ*, 345, 245
- Carretta, E., & Gratton, R. G. 1997, *A&AS*, 121, 95
- Carretta, E., Gratton, R. G., Clementini, G. & Fusi Pecci, F. 2000, *ApJ*, 533, 235
- Casertano et al. 2000, *AJ*, 120, 2747
- Cassisi, S. Castellani, M., Caputo, F., & Castellani, V. 2004, *A&A*, 426, 641
- Castellani, V. & Quarta, M. L. 1987, *A&AS*, 71, 1
- Chaboyer, B., Demarque, P., Kernan, P. J., & Krauss, L. M. 1998, *ApJ*, 494, 96
- Cohen, J.G. & Matthews, K. 1992, *PASP*, 104, 1205
- Cool, A. M., Piotto, G., & King, I. R. 1996, *ApJ*, 468, 655
- Dean, J. F., Warren, P. R., & Cousins, A. W. J. 1978, *MNRAS*, 183, 569
- Di Marchi, G. & Paresce, F. 195, *A&A*, 304, 202
- Dolphin, A. E. 2000, *PASP*, 112, 1397
- Elias, J. H., Frogel, J. A., Matthews, K., & Neugebauer, G. 1982, *AJ*, 87, 1029
- Elson, R. A. W., Gilmore, G. F., Santiago, B. X., & Casertano, S. 1995, *AJ*, 110, 682
- Girardi, L., Bertelli, G., Bressan, A., Chiosi, C., Groenewegen, M. A. T., Marigo, P., Salasnich, B., & Weiss, A. 2002, *A&A*, 391, 195
- Gratton, R. G., Carretta, E., Claudi, R., Lucatello, S., & Barbieri, M. 2003, *A&A*, 404, 187

- Hansen, B. M. S., et al. 2004, *ApJS*, 155, 551
- Harris, W. E. 1996, *AJ*, 112, 1487
- Jefferys, W. H., Fitzpatrick, M. J., & McArthur, B. E. 1988, *Celestial Mechanics*, 41, 39
- Kaluzny, J., Olech, A., Thompson, I., Pych, W., Krzeminski, W. & Schwarzenberg-Czerny, A. 1999, *A&AS*, 143, 215
- King, I. R., Anderson, J., Cool, A. M., & Piotto, G. 1998, *ApJ*, 492, L37
- Kovacs, G. & Walker, A. R. 2001, *A&A*, 374, 264
- Landolt, A. U. 1992, *AJ*, 104, 340
- Longmore, A. J., Dixon, R., Skillen, I., Jameson, R. F., & Fernley, J. A. 1990, *MNRAS*, 247, 684
- Marconi, M., Caputo, F., Di Criscienzo, M., Castellani, M. 2003, *ApJ*, 596, 299
- Reid, I. N. 1996, *MNRAS*, 278, 367
- Reid, I. N. 1998, *AJ*, 115, 204
- Renzini, A., Bragaglia, A., Ferraro, F. R., Gilmozzi, R., Ortolani, S., Holberg, J. B., Liebert, J., Wesemael, F., & Bohlin, R. C. 1996, *ApJ*, 465, L23
- Renzini, A. & Fusi Pecci, F. 1988, *ARA&A*, 26, 199
- Richer, H. et al. 1995, *ApJ*, 451, L17
- Richer, H. et al. 1997, *ApJ*, 484, 741
- Sandquist, E. L., Bolte, M., Langer, G. E., Hesser, J. E., Mendes de Oliveira, C. 1999, *ApJ*, 518, 262
- Sarajedini, A., Geisler, D., Schommer, R., & Harding, P. 2000, *AJ*, 120, 2437
- Schlegel, D. J., Finkbeiner, D. P., Davis, M. 1998, *ApJ*, 500, 525
- Silbermann et al. 1996, *ApJ*, 470, 1
- Stetson, P. B. 1994, *PASP*, 106, 250
- Stetson, P. B. 2000, *PASP*, 112, 925

- Storm, J., Carney, B.W. & Beck, J.A. 1991, *PASP*, 103, 1264
- Storm, J., Carney, B.W. & Latham, D.W. 1992, *PASP*, 104, 159
- Testa, V., Chieffi, A., Limongi, M., Andreuzzi, G., & Marconi, G. 2004, *A&A*, 421, 603
- Turner, A. 1996, “ALLFRAME Cookbook”.
- Williams, R. E., et al. 1996, *AJ*, 112, 1335
- Wood, M. A. 1995, in *White Dwarfs*, ed. D. Koester & K. Werner (Berlin: Springer), 41
- Zoccali, M., et al. 2001, *ApJ*, 553, 733

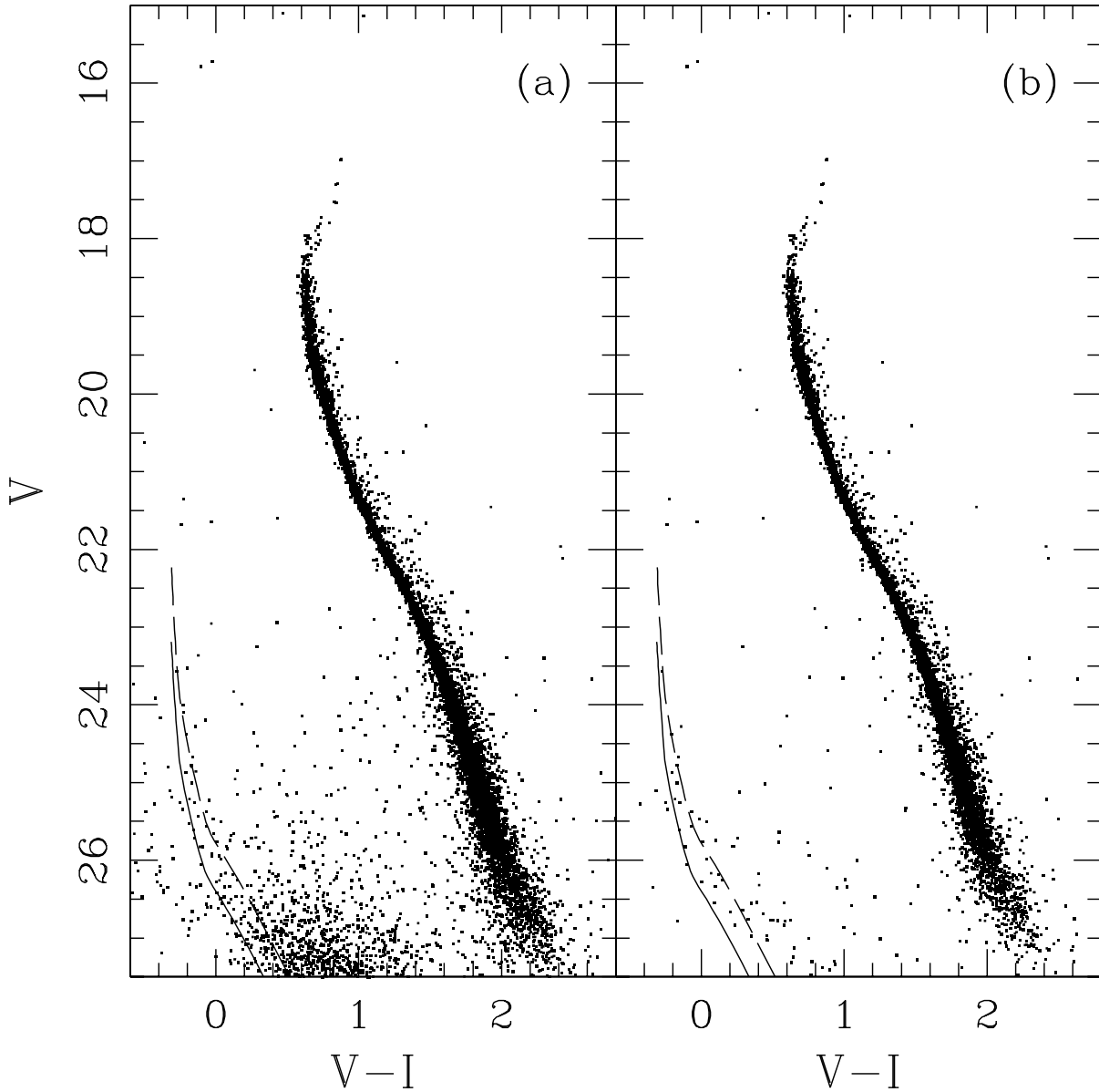


Fig. 1.— The calibrated, VI CMD for M5. (a) All objects from Table 2 are plotted as dots. The dashed and solid lines represent the WD cooling tracks of Bergeron et al. (1995) for $\log(g) = 7.5$ and 8.0 respectively, shifted to a distance modulus of $(m - M)_0 = 14.67$ mag and reddening of $E(V - I) = 0.046$ mag. (b) Only objects classified as stellar (see Sec. 2.3) are plotted.

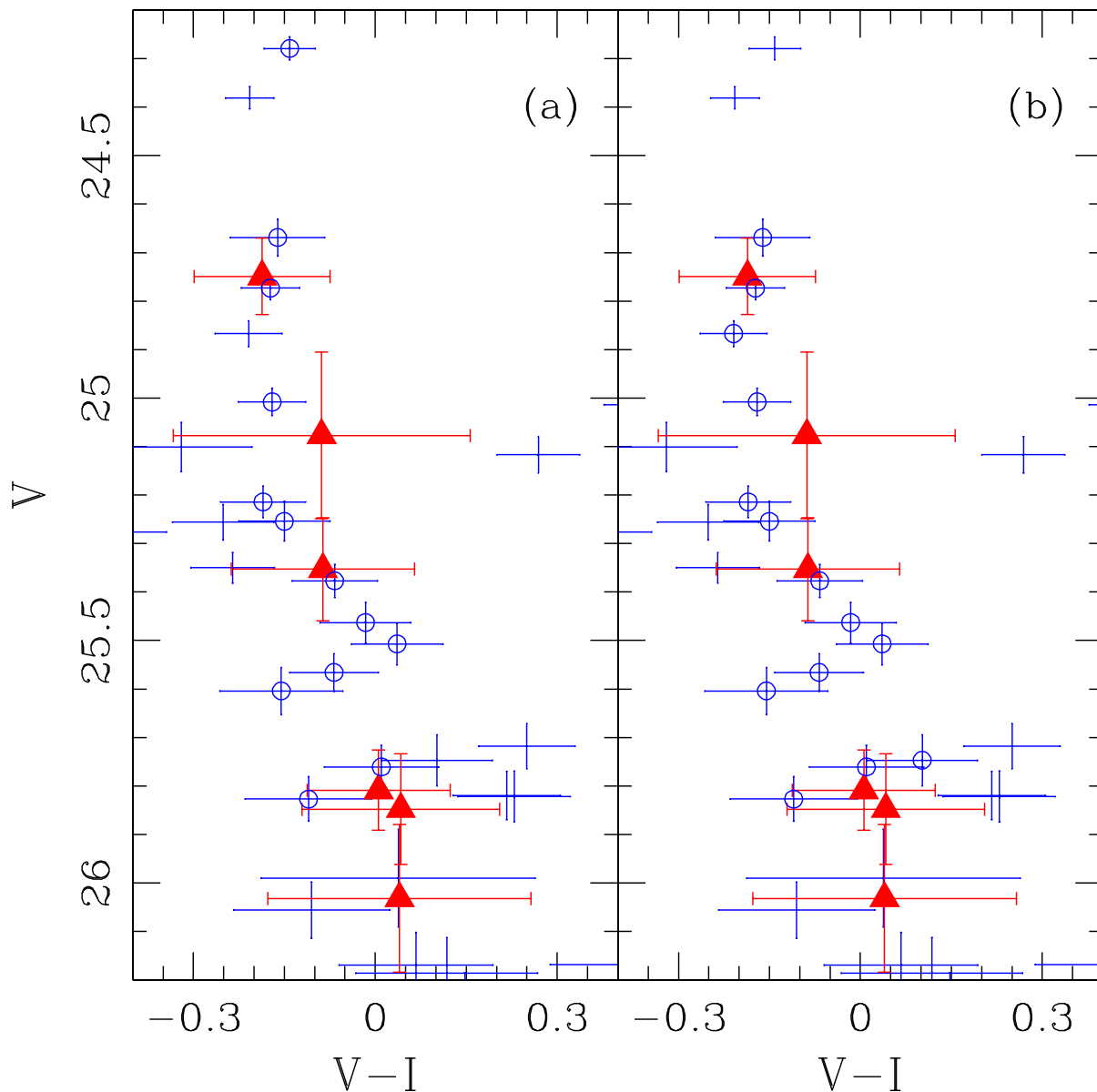


Fig. 2.— The WD region of the M5 CMD showing the WDs used (open circles) and not used (bare error bars) in the distance fits in Sec. 3. The calibrating field WDs, shifted to the fitted distance modulus of M5, are shown as triangles. Panel (a) shows the results of the first-pass fit, while (b) is for the reselected WD candidates used in the second pass distance determination.

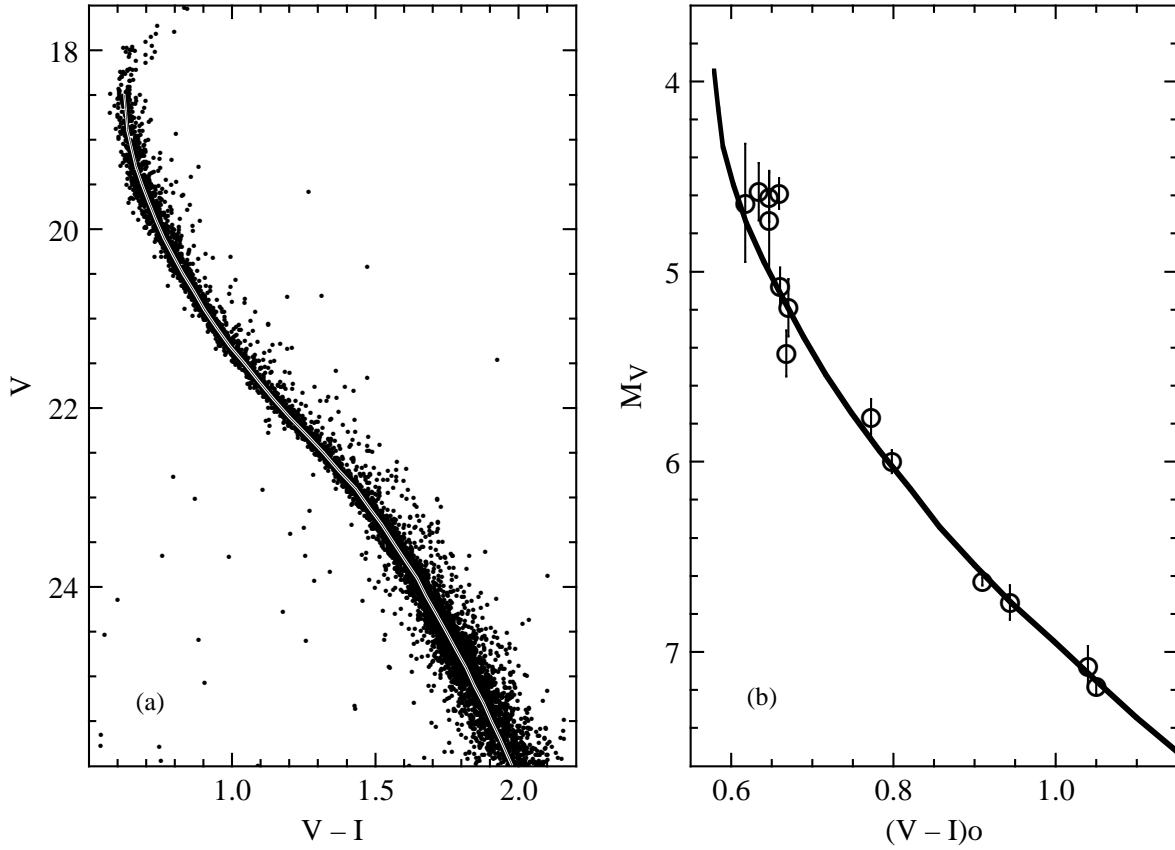


Fig. 3.— The CMD in panel (a) shows the M5 fiducial main sequence plotted over the stars. In panel (b), we show the weighted least squares fit of the M5 fiducial main sequence (solid line) to the field subdwarfs with *Hipparcos* parallaxes (open circles). The adopted reddening and metallicity, along with the derived distance modulus, are discussed in Sec. 4.

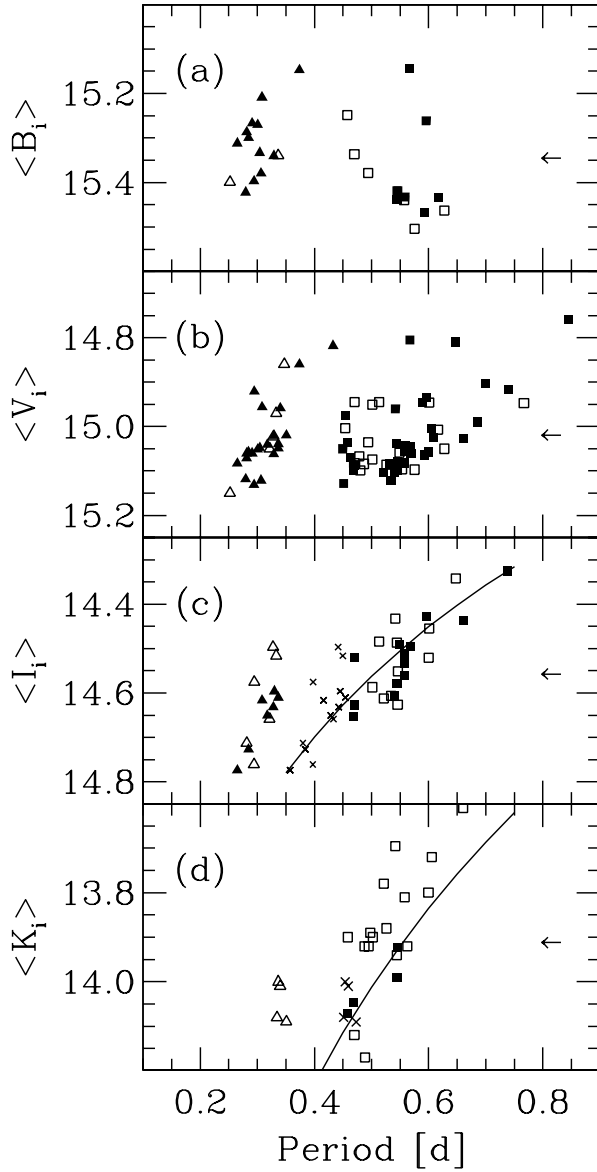


Fig. 4.— Apparent magnitudes of RRL in M5 compiled from the literature, plotted as a function of pulsation period, for the B , V , I , and K passbands. In each figure, the arrow indicates the mean apparent magnitude of the RRL. Squares and triangles indicate RRab and RRC pulsators, respectively. Solid symbols indicate stars with light curves having complete phase coverage, while open symbols indicate stars with small phase gaps. The crosses in (c) and (d) indicate the fundamentalized positions of the RRC stars, while the curves are the best fits represented by the coefficients in lines 1 and 2 of Table 5.

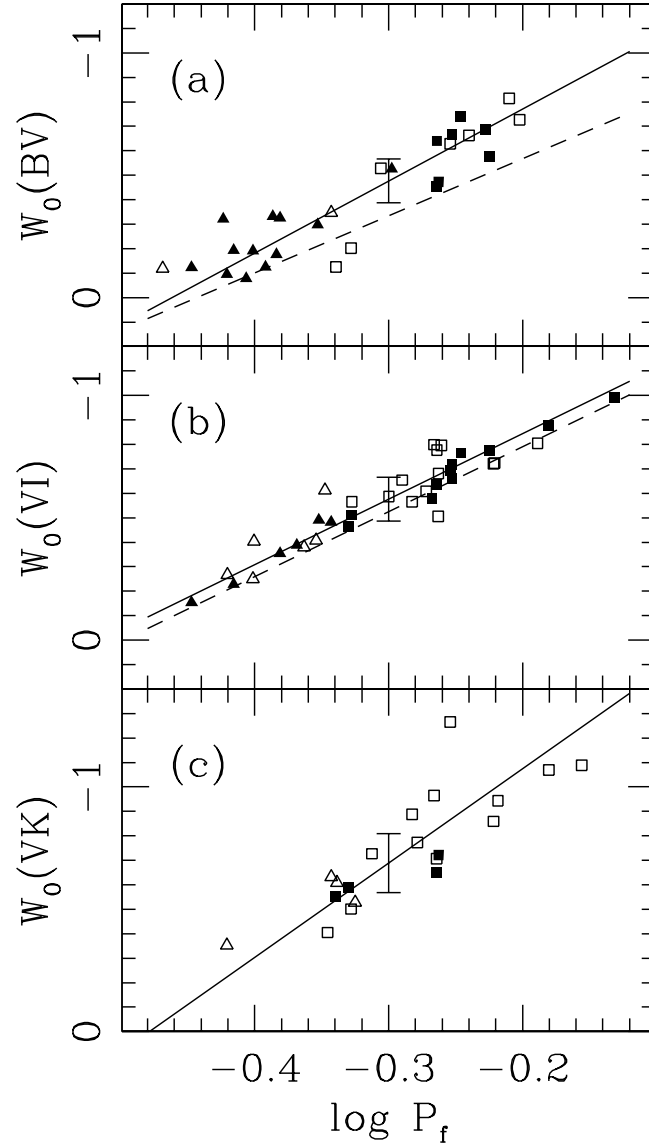


Fig. 5.— Wasenheit functions for the M5 RRL as a function of fundamentalized period. The symbols are as in Figure 4. Solid lines represent our least-squares fits to the data, while dashed lines indicate the predictions of models by Cassisi et al. (2004). Error bars indicate systematic uncertainty in the fit due to uncertainties in the distance modulus and photometric zeropoints.

Table 1. Observation Log.

Visit	Date	N_{orbit}	Filter	Exposures
1	1999 Jul 25	1	F814W	2×700 sec, 600 sec, 60 sec, 5 sec
		2	F555W	3×700 sec, 60 sec, 5 sec
		3	F814W	3×800 sec
		4	F555W	3×800 sec
2	1999 Aug 9	1	F814W	2×700 sec, 600 sec, 60 sec, 5 sec
		2	F555W	3×700 sec, 60 sec, 5 sec
		3	F814W	3×800 sec
		4	F555W	3×800 sec
3	1999 Jul 29	1	F814W	2×700 sec, 600 sec, 60 sec, 5 sec
		2	F555W	3×700 sec, 60 sec, 5 sec
		3	F814W	3×800 sec
		4	F555W	3×800 sec
4	1999 Jul 17	1	F814W	2×700 sec, 600 sec, 60 sec, 5 sec
		2	F814W	3×800 sec
		3	F814W	3×800 sec

Table 2. WFPC2 Photometry.

ID	WF	X	Y	V	ϵ_V	I	ϵ_I	ellip	fwhm	class
1	2	179.08	26.53	24.885	0.046	23.162	0.027	0.518	6.60	0.62
3	2	244.22	27.58	24.873	0.057	22.177	0.032	0.060	2.71	0.03
4	2	280.22	27.98	22.112	0.025	20.858	0.023	0.340	1.62	0.98
5	2	115.19	28.21	22.939	0.019	21.517	0.015	0.389	2.18	0.93
...
1	3	67.80	47.25	25.248	0.067	23.444	0.031	0.348	0.77	1.00
2	3	110.09	48.82	23.441	0.023	21.966	0.018	0.436	1.39	0.93
3	3	128.82	48.98	25.153	0.049	23.410	0.028	0.039	1.07	0.99
4	3	554.64	49.04	24.620	0.061	22.939	0.031	0.270	12.37	0.04
...
1	4	768.48	42.40	24.820	0.035	23.039	0.022	0.183	2.06	0.16
2	4	674.81	42.46	24.657	0.042	22.892	0.028	0.201	2.88	0.02
3	4	599.91	43.10	23.487	0.021	21.951	0.021	0.186	2.27	0.58
4	4	561.39	43.15	21.601	0.019	21.170	0.016	0.133	1.56	0.99

Note. — The complete version of this table is in the electronic edition of the Journal. The printed edition contains only a sample.

Table 3. Photometry of Field White Dwarfs.

Star	V	ϵ_V	$V - I$	ϵ_{V-I}
WD 0644+375	9.96	0.08	-0.23	0.11
WD 1327-083	10.56	0.11	-0.13	0.15
WD 1935+327	11.06	0.11	0.00	0.16
WD 2126+734	10.29	0.17	-0.13	0.25
WD 2326+049	11.24	0.15	0.00	0.22
WD 2341+322	11.02	0.08	-0.03	0.12

Table 4. M5 RR Lyrae Magnitudes.

Sample	N_{RR}	$m(RR)$	sem	σ	median	$M(RR)$
V -band, all	79	15.024	0.009	0.082	15.05	$+0.42 \pm 0.10$
V -band, RRab	53	15.025	0.011	0.082	15.05	$+0.42 \pm 0.10$
V -band, RRC	26	15.023	0.017	0.084	15.05	$+0.42 \pm 0.10$
B -band, all	28	15.350	0.018	0.095	15.36	$+0.71 \pm 0.10$
B -band, RRab	14	15.385	0.027	0.102	15.43	$+0.74 \pm 0.10$
B -band, RRC	14	15.314	0.020	0.076	15.32	$+0.67 \pm 0.10$
I -band, all	37	14.562	0.017	0.104	14.58	$+0.00 \pm 0.10$
I -band, RRab	24	14.520	0.018	0.087	14.52	-0.04 ± 0.10
I -band, RRC	13	14.641	0.024	0.086	14.63	$+0.08 \pm 0.10$
K -band, all	28	13.917	0.036	0.191	13.92	-0.59 ± 0.12
K -band, RRab	23	13.880	0.039	0.188	13.90	-0.63 ± 0.12
K -band, RRC	5	14.086	0.045	0.100	14.08	-0.42 ± 0.12

Table 5. Results of Period-Magnitude Fits.

Line	Function	a	b	rms	N_{RR}	R
1	$I(RR)$	14.56 ± 0.01	-1.40 ± 0.10	0.05	36	–
2	$K(RR)$	14.01 ± 0.02	-2.23 ± 0.05	0.04	4	–
3	$M_I(RR)$	0.00 ± 0.10	-1.40 ± 0.10	0.05	36	–
4	$M_K(RR)$	-0.50 ± 0.12	-2.23 ± 0.05	0.04	4	–
5	$W_0(BV)$	-0.48 ± 0.10	-2.94 ± 0.24	0.10	28	3.10
6	$W_0(VI)$	-0.58 ± 0.10	-2.68 ± 0.15	0.07	36	2.39
7	$W_0(VI)$	-0.65 ± 0.10	-2.82 ± 0.16	0.07	36	2.54 ^a
8	$W_0(VK)$	-0.69 ± 0.10	-3.85 ± 0.49	0.14	20	0.13

^aFor comparison with models of Cassisi et al. (2004).